Chemical Geology xxx (2016) xxx–xxx

Contents lists available at ScienceDirect

Chemical Geology

journal homepage: www.elsevier.com/locate/chemgeo

An experimental simulation of volcanic ash deposition in gas turbines and implications for jet engine safety

Christopher Giehl [a,b,*], Richard A. Brooker [a,c], Holger Marxer [a], Marcus Nowak [a]

[a] Department of Geosciences, University of Tübingen, 72074 Tübingen, Germany
[b] Institute of Geosciences, Christian-Albrechts-University Kiel, 24118 Kiel, Germany
[c] School of Earth Sciences, University of Bristol, Bristol BS8 1RJ, UK

ARTICLE INFO

Article history:
Received 11 March 2016
Received in revised form 13 November 2016
Accepted 16 November 2016
Available online xxxx

Keywords:
Volcanic ash
Turbine blades
Nickel superalloy
Thermal barrier coating
Wetting behaviour
Melting temperature
Glass transition temperature

ABSTRACT

The protracted grounding of commercial aircraft throughout Europe due to the Eyjafjallajökull volcanic eruption in Iceland April 2010, has alerted the public to the potential dangers of aircraft encounters with ash clouds. One of the most serious issues is the failure of jet turbines due to the deposition of molten silicate ash particles on hot turbine components. In this study, we highlight the influence of volcanic ash composition, crystal/glass ratio and resulting bulk viscosity on the interaction of ash particles with hot turbine blades and vanes.

A range of volcanic materials are used to simulate ash melting during transport through the combustor and deposition on a turbine blade of nickel superalloy material commonly used for the hot components in jet engines. The results show how 'on-blade' accumulation of molten particles can lead to efficient adhesion (wetting) and subsequent rapid accumulation of further molten material in some circumstances. In other cases particles form a cinder-like layer or entirely bounce off the blade. Any deposits will disrupt the air flow in the turbine, clog the cooling system and eventually cause the engine to stall. However, the cinder deposits can be removed in our experiments (as well as 'in-flight' for a real engine) by shutting off the heat source, allowing the deposit to quench and dislodge by thermal stress cracking. However, this currently recommended airplane safety procedure will not work for more basaltic melts which wet the blade surface more efficiently. Our experiments demonstrate how the nature of the incoming ash particle strongly influences the type of deposit formed, the important parameters being bulk ash composition, crystal proportion and particle size.

1. Introduction

The lengthy shut down of European aviation due to the ash erupted in April 2010 from Icelandic Eyjafjallajökull Volcano has made the public painfully aware of the consequences that volcanic ash may have for airline travel. This disruption had significant economic consequences, with 108,000 flights being cancelled, 10 million passengers stranded and an estimated revenue loss of US $ 1.7 billion in the first six days of the eruption (IATA Economic Briefing, 2010; Budd et al., 2011). There have been questions and recriminations regarding the actual hazards involved and the need for such drastic action (Brooker, 2010; Clarkson et al., 2016). Since 1973 there have been >100 reported encounters of jet aircraft with volcanic ash and nine encounters with temporary engine failure that required 'in-flight' restart of engine (Guffanti, 2004; Guffanti et al., 2010). Many other serious incidents go unreported (e.g. Casadevall, 1994; Christmann et al., 2015). Some of the well-documented, high profile incidents along with the volcanoes involved are listed in Table 1 (more detailed descriptions can be found in eSupp. 1). This includes the most severe encounters where coatings of melted ash on hot turbine parts were reported. (see also Hanstrum and Watson, 1983; Przedpelski and Casadevall, 1994; Dunn et al., 1996; Grindle and Burcham, 2003; Dunn, 2012; Davison and Rutke, 2014).

Ash compositions reported in Table 1 cover a range from basaltic to rhyolitic, typically with variable proportions of glass and crystal fragments (see Table 1 for references). It is well known that silicate glass composition, (especially SiO_2 content) exerts major controls on melting temperature and other physical properties of melts. However, monitoring of volcanic ash clouds for aircraft safety is mostly concerned with particle concentration and grain size (e.g. Watson and Oppenheimer, 2001; Witham et al., 2011), not composition. Even some general idea of the erupted bulk magma composition may hide some important detail. For instance, the majority of volcanic ash erupted from Eyjafjallajökull in 2010 was andesitic and dominated by glass (Gislason et al., 2011), with crystal proportions varying from 10 to 30% (Cioni et al., 2014). However, there was also an additional, more basaltic component (Sigmarsson et al., 2011). Also, volcanic ashes at greater distance from a vent can have a higher proportion of glass fragments due to their greater persistence in the ash cloud compared to denser and

---

* Corresponding author at: Institute of Geosciences, Christian-Albrechts-University Kiel, 24118 Kiel, Germany.
E-mail address: christopher.giehl@min.uni-kiel.de (C. Giehl).

http://dx.doi.org/10.1016/j.chemgeo.2016.11.024
0009-2541/© 2016 Elsevier B.V. All rights reserved.

Please cite this article as: Giehl, C., et al., An experimental simulation of volcanic ash deposition in gas turbines and implications for jet engine safety, Chem. Geol. (2016), http://dx.doi.org/10.1016/j.chemgeo.2016.11.024

Table 1
Jet aircraft encounters with volcanic ash.

Volcano	Ash composition	Year	Damage to turbine
Mt St. Helens (USA)	Dacitic (Taylor and Lichte, 1980)	1980	Accumulation of ash and glass (Kim et al., 1993)
Mt Galunggung (Indonesia)	Basaltic (Harmon and Gerbe, 1992)	1982	Massive accumulation of ash and glass, turbines stalled, successful restart (Hanstrum and Watson, 1983; Campbell, 1990; Chambers, 1985)
Soputan (Indonesia)	High Alumina Basalt (Kushendratno et al., 2012)	1985	Observations of St Elmo's fire and dust in cabin. 747 had all four engines damaged (Guffanti et al., 2010)
Redoubt (USA)	Andesitic (Swanson et al., 1994)	1989	Accumulation of ash, turbines failed but were restarted successfully (Steenblik, 1990; Casadevall, 1994)
Mt Pinatubo (Philippines)	Dacitic (Wiesner et al., 1995)	1991	Blocked cooling holes and coatings on blades (Dunn et al., 1996; Casadevall et al., 1999)
Hekla (Iceland)	Andesitic (Olafssdottir and Sigmundsson, 2001)	2000	Blocked cooling holes, build-up of fine ash in passages, blistered thermal barrier coatings and blade abrasion (Pieri et al., 2002; Grindle and Burcham, 2003)
Manam (Papua New Guinea)	Basaltic (Johnson et al., 1985)	2006	Gulfstream II twin-engine flame-out. Both engines were restarted following descent (Tupper et al., 2007)
Eyjafjallajökull (Iceland)	Andesitic with basaltic & rhyolitic components (Gislason et al., 2011; Sigmarsson et al., 2011)	2010	Two weeks no fly zone in Europe, no incidents (Brooker, 2010)
Kelut (Indonesia)	Probably andesitic?	2014	A320 landed safely but had damage to engine (Clarkson et al., 2016)

mostly larger mineral fragments (e.g. Sparks and Walker, 1977). Even when ash samples are immediately collected on the ground or measured in-situ with airborne methods, the crystal/glass ratios in a distant cloud are very difficult to predict. As this study will show, all these variables will affect ash deposition in jet engines.

1.1. Engine design

To designing experiments that simulate ash ingestion it is first important to understand the operation principle of jet turbines (Koff, 2004; Rolls-Royce, 1996). A modern bypass engine consists of four main units (1–4) as illustrated in Fig. 1a. The first unit is the turbo fan (1) that generates about 75% of the engine thrust, and can force 300 m^3 air per second into the engine equivalent to ~110 kg/s dry air at 11 km altitude cruising level. Even for lower limit ash cloud encounters this airflow can rapidly introduce a large amount of material. The 2010 European Commission 'safe to fly' ash limit of 4 mg/m^3 gives 0.72 kg of ash ingestion in 10 min. About ~10–20% (e.g. Rolls Royce Trent 1000 or Trent 700) of this incoming air is diverted into the compressor (2) before being ignited with fuel in the combustion chamber (3) and expanding to driving the turbine (4). The combusted air driving the turbine (4) is typically at ~1200–1350 °C in older engines, but up to 1575 °C in modern turbofan engines during take-off and climb (Fig. 1b). The high temperature turbine components of modern engines (nozzle, vanes, and turbine blades) are made of nickel superalloy (NSA) (e.g. Inconel 713LC) which has a melting point in the range of 1260–1288 °C, lower than the maximum combustion temperature. This is facilitated by air-film cooling of the metal using a system of mm-sized holes in the vanes and turbine blades (Fig. 2) fed by air channels from the compressor (2).

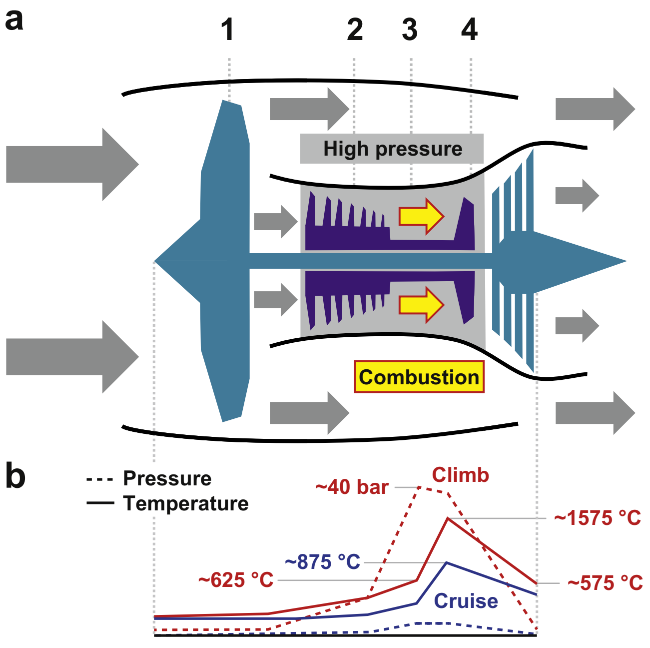

Fig. 1. (a) Schematic cross-section of a turbofan-engine, 1 = turbofan, 2 = compressor, 3 = combustor, 4 = turbine. (b) The typical operating temperatures and pressures reached during cruise and climb are shown for the various engine parts (Rolls Royce circa 2015; provided courtesy Rory Clarkson).

It is clearly possible that a volcanic ash particle passing through the combustion unit (3) can be exposed to temperatures well above its liquidus temperature (800–1200 °C) and might therefore be molten by the time it reaches the turbine blades (4) even if these are cooled to a lower temperature. These particles can clog the cooling system and cause turbine failure (Dunn et al., 1996) or at the very least disrupt the carefully designed airflow causing overheating, burner pressure increase, imbalance in the fuel-air mixture or carbon build-up on combustor fuel nozzles and stalling of the engine (e.g. Przedpelski and Casadevall, 1994; Dunn et al., 1996; Grindle and Burcham, 2003; Dunn, 2012; Davison and Rutke, 2014). As a result, the melting kinetics and adhesion behaviour of molten or partially molten volcanic ash particles on the turbine blades, are crucial parameters to consider during an ash cloud encounter.

Ceramic thermal barrier coatings (TBC's) have also recently been developed to 'insulate' the metal blade, allowing a further increase in turbine operating temperatures (Fig. 2). TBC's are refractory-oxide ceramic coatings applied to the surfaces of metallic parts in the hottest part of jet engines, typically made of 7 wt.% Y_2O_3-stabilized ZrO_2 (7YSZ) ceramics (Padture et al., 2002). However, there are still many older aircraft operating with 'bare' NSA blades (Grindle and Burcham, 2003) and it has been shown that silicate melt deposits can also corrode and destroy the thin TBC layer and expose the NSA to the extreme operational temperatures and successive ash particles (Grindle and Burcham, 2003; Krämer et al., 2006; Drexler et al., 2011; Vidal-Setif et al., 2012). As a result, experiments simulating ash interaction with NSA material are still essential and form a technical basis for further work on TBC's and new materials such as silicon carbide based ceramic matrix composites (CMC) in the next generation of jet engines.

1.2. Previous testing and research

In the past, gas turbine engines were tested for the effect of ingestion of solid particles according to the procedures of Military Specification MIL-E-5007D, commonly known as the 'Arizona road-dust test' (Dunn

Please cite this article as: Giehl, C., et al., An experimental simulation of volcanic ash deposition in gas turbines and implications for jet engine safety, Chem. Geol. (2016), http://dx.doi.org/10.1016/j.chemgeo.2016.11.024

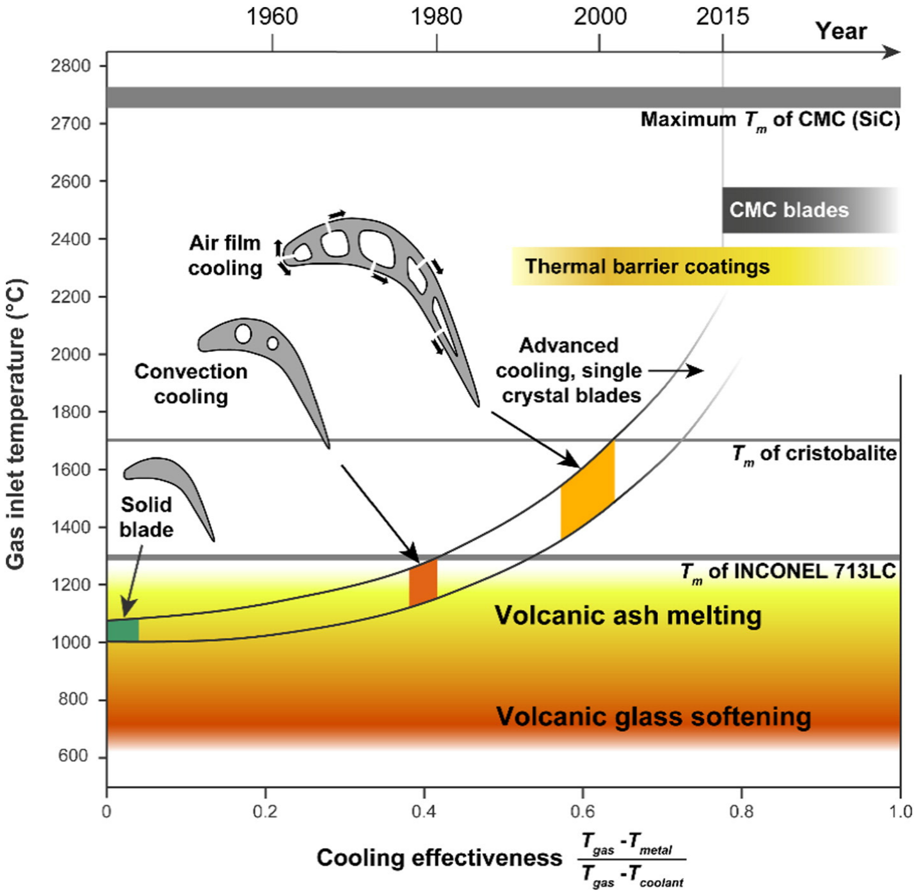

Fig. 2. Development of turbine blade running temperatures and design. Modified after Koff (2004). Note the development of an internal air feed system and air film cooling in the blades operating above their melting point. The small arrows represent the flow of this air film. The melting range (T_m) or the softening point (the glass transition T_g) for silicate glasses are indicated along with the melting point of cristobalite, the high temperature form of quartz (i.e. sand).

et al., 1996). However, it is unclear if this standard uses quartz sand or in fact a mixture of volcanic and other silicate materials as defined by Kim et al. (1993). This mixture bears little resemblance to volcanic ash and it is important to note (in contrast to Davison and Rutke, 2014) that a similar bulk chemical composition is no guarantee that it will react in the same way as ash which has totally different constituent materials. Dunn et al. (1996) claim that just prior to 1996, the material used in this standard was changed to be pure quartz, even though Smialek et al. (1994) had already noted that the severity of NSA turbine blade degradation is controlled by different ash compositions. It remains unclear if anything other than quartz with 1000–75 μm grain size was ever used and in any case this standard was dropped by 1997. Without doubt, sandstorm encounters are a severe hazard to aviation leading to erosion, attrition and clogging of the cooling system in the colder parts of the engines (Grindle and Burcham, 2003) resulting in overheating, burner pressure increase, imbalance in the fuel-air mixture or carbon build-up on combustor fuel nozzles (e.g. Brun et al., 2012; Davison and Rutke, 2014). However, the physico-chemical properties of quartz are very different to the vast range of more common volcanic silicate minerals and silicate glass compositions. This compositional range is also ignored in other studies that assume constant melting temperatures for volcanic ash (~827 °C, Vogel et al., 2011).

Published results on the effects of volcanic ash in aviation jet engines are limited to a few studies in the early 1990s, perhaps as a consequence of incidents in the 1980s listed in Table 1. Kim et al. (1993) investigated the ingestion of different 'ash' compositions, but most of the experiments were performed with unrealistic mixtures of basalt lava quarried for ornamental stone, clays (to introduce a particle size range) and 'soil', materials used in the construction and horticultural industries. A few experiments with Mt St. Helens ash and pure basaltic lava using partial engines (no compressor) were not given high prominence. Publications include pictures of the actual deposits formed on the vanes and turbine after stripping down the 'engine'. The only published study using actual, complete jet engines (Dunn et al., 1996) reports the effect on the engine performance as ash (Mt St. Helens ash with 25% glass and soil blend with black scoria) deposits accumulate, but lacks detailed description of the formed deposits.

After the April 2010 Eyjafjallajökull eruption a new series of publications addressed the issue. Mechnich et al. (2011) studied the interaction of a TBC with volcanic ash from Eiyafjällajökull. Wetting and corrosion were observed at relatively low temperatures of 930–1100 °C and negative effects on thermal insulation and thermal cycling behaviour were observed. In contrast, similar experiments with modified coatings by Drexler et al. (2011) suggest that recrystallization of sticking ash can act as a barrier preventing further penetration of molten material. Preliminary results of our study (Nowak et al., 2011, 2013; Giehl et al., 2016) indicated, for the first time, the importance of the crystal/glass ratio for the wetting efficiency of volcanic ash on NSA in addition to particle size, glass proportion, and turbine blade temperature. Dunn (2012) reached similar conclusions and stated that the airline community needs to rapidly acquire information on the calcium content of newly erupted volcanic material. This statement illustrates the need for a simple, but well researched and robust volcanic ash classification that can be easily applied to ongoing eruptions. More recently, Kueppers et al. (2014) compared the sintering behaviour of commonly used test sand (quartz and silicate mineral mixtures) and Eyjafjallajökull ash heated in Ca-phosphate crucibles with complete sintering of the volcanic ash occurring at relatively low temperatures (1050 °C) required for

Please cite this article as: Giehl, C., et al., An experimental simulation of volcanic ash deposition in gas turbines and implications for jet engine safety, Chem. Geol. (2016), http://dx.doi.org/10.1016/j.chemgeo.2016.11.024

mixtures of silicate minerals, including quartz. Static experiments by Song et al. (2014, 2016) have shown the manner of adhesion and wetting by heating a block of compacted ash placed on a Al_2O_3 substrate. In a design that partly emulated the experimental set up in this study, Taltavull et al. (2016) illustrate how particle size, impact angle, speed and temperature can affect the adhesion of basaltic ash onto a stainless steel target. They concur with Nowak et al. (2011, 2013) that the glass component and its pre-melting softening temperature (the glass transition T_g) might be important. In a related study, Dean et al. (2016) suggest there are subtle variations in adhesion properties amongst a compositional range of basaltic ashes, possibly related to variation in viscosity.

In summary, there is an increasing awareness that the amount of glass in the ash cloud could be a critical parameter for turbine engine failure by adhesion and wetting. Although ash melting, adhesion, and wetting are kinetically controlled by travel and dwell time in the turbine hot section (e.g. Taltavull et al., 2016), there are no detailed dynamic studies of ash interaction with turbines that cover a realistic range of ash composition combined with realistic turbine thermal profiles.

2. Materials and methods

2.1. Volcanic materials

Volcanic 'ashes' with compositions ranging from low-SiO_2 basalt to high-SiO_2 rhyolite (Table 2, Le Bas and Streckeisen, 1991), were prepared from volcanic rocks. Crystalline quartz (sand) was also used in a few experiments. Crystal proportions in ash experiments were selected by grinding partially crystalline rocks. Homogeneous glasses were synthesised by melting the rock samples in air for 1 h at 1200 °C (rhyolite), 0.5 h at 1300 °C (basalt), and 0.5 h at 1400 °C (andesite, dacite) in graphite crucibles and quenching in water. The starting materials were ground and separated by sieving into grain size fractions of 500–300, 300–200, 200–125, 125–63, 125–5 and <63 μm. Some materials were taken to <50 μm, but the sieving process tends to fractionate the glass from the different minerals and results in modified bulk composition. We therefore used the 125–5 μm mixtures to represent the finer particles that get milled in the turbofan and compressor. Several pieces of basaltic and rhyolitic glass and selected experimental products were mounted in epoxy, carbon-coated and subsequently characterized by back-scattered electron images and electron microprobe analysis (see eSupp. 1 for analytical details). Characteristics of starting material (composition, observed minerals and crystal proportion) are included in Table 2.

Table 2
Studied volcanic ask bulk compositions.

wt.%	Basalt[a]	Andesite[b,c]	Dacite[b,d]	Rhyolite[a]
SiO_2	52.0 (7)	53.91	63.7	73.4 (1.7)
TiO_2	2.8 (1)	1.02	0.8	0.9 (1)
Al_2O_3	13.0 (2)	18.65	13.5	11.9 (3)
FeO^*	12.4 (9)	7.36	7.8	2.8 (4)
MnO	0.2 (1)	0.13	0.2	0.1 (1)
MgO	5.9 (2)	5.55	0.8	1.0 (2)
CaO	10.2 (1)	8.83	3.7	2.9 (1.2)
Na_2O	3.0 (2)	3.67	4.4	6.4 (9)
K_2O	0.5 (0)	0.68	2.4	2.4 (1)
P_2O_5	0.3 (0)	0.19	0.1	0.2 (1)
Total	100.2	100.0	97.4	101.8
Observed minerals	Olivine + plagioclase	Olivine + plagioclase	Plagioclase	Opaque crystals
Crystal proportion[e] (%)	40	60	>95	<5
Calculated viscosity of melt with respective composition[f] (log Pa·s)				
1250 °C	1.6	1.7	3.2	3.8
1500 °C	0.3	0.4	1.9	2.4

(x) = 0 · x = 1σ standard deviation of the mean, total iron reported as FeO^*.
[a] Remelted and quenched glass analyzed with electron microprobe (n = 10).
[b] Whole-rock X-ray fluorescence analysis.
[c] Schmidt and Grunder (2009).
[d] Walker (1963).
[e] Unmelted crushed rock powders, the crystal proportion was determined with polarisation microscopy using immersion mounts.
[f] Viscosities calculated after Giordano et al. (2008), assuming 0.2 wt.% H_2O.

2.2. Experimental design

In this study a particle size range of 500–5 μm is used to represent a distribution of volcanic eruptive products. The larger particles (>250 μm) are unlikely to persist in ash clouds for >10 km from the volcano (Bursik et al., 1991; Davison and Rutke, 2014), but are useful in understanding particle-melting kinetics. It should be noted that efficient particle size reduction of different siliceous debris (airborne dust, sand, natural and fossil ash) in the turbine compressor has been shown to give typical particle sizes of 6 μm with significant amounts below 4 μm (Clarkson et al., 2016), but particles <3 μm might be expected to flow around obstacles rather than impact them (Taltavull et al., 2016). The various size fractions of different materials (and quartz) were fed into the experimental setup (Fig. 3) representing a simplified turbine hot section. The different starting materials were dropped into the hot part of a rapid flowing acetylene-oxygen micro-torch flame (the 'combustor', Fig. 1a) which accelerates the particles towards a NSA target blade (Inconel 713LC). An Al_2O_3 tube was used to feed approximately 0.5 to 1 g of powder into the flame over 30 to 120 s. The mildly oxidizing torch flame was directed at the unsupported end of the NSA sheets (0.5 mm thickness, 30/60 mm length, and 10 mm width) at an angle of 45°. Particles were fed into the hot gas stream about 10 to 20 mm after the tip of the flame hot spot. As a deposit builds up (Fig. 3, see Section 3.3), the particle transport, impact, dwell time, adhesion and wetting behaviour on the target were documented by microscope-assisted digital video (DV) recording at high temporal

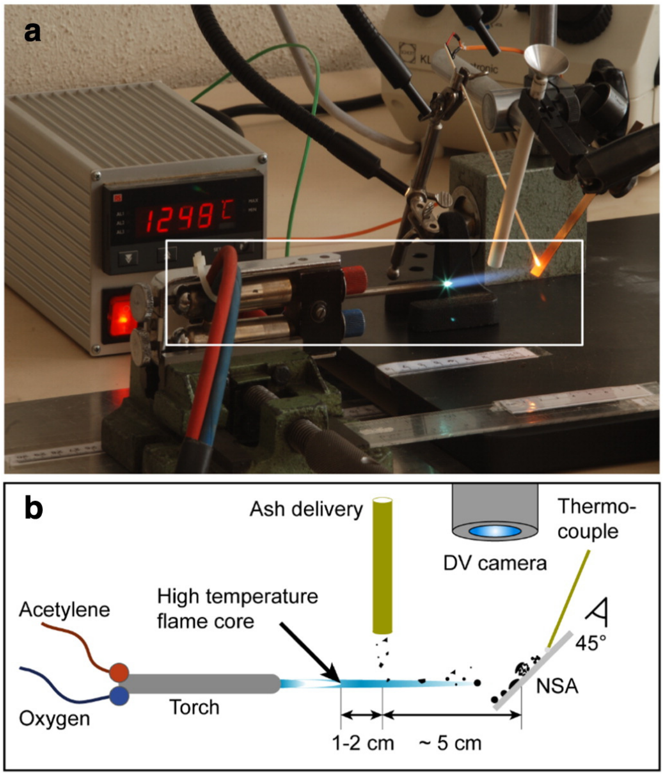

Fig. 3. (a) Photograph of the experimental setup: acetylene-oxygen micro-torch, ash delivery tube, NSA blade target and S-type thermocouple. (b) Schematic sketch of the experimental setup outlined in (a).

Please cite this article as: Giehl, C., et al., An experimental simulation of volcanic ash deposition in gas turbines and implications for jet engine safety, Chem. Geol. (2016), http://dx.doi.org/10.1016/j.chemgeo.2016.11.024

resolution. The temperature at the impact site was monitored by a S-Type (PtRh) thermocouple (Fig. 3). A constant and realistic NSA target surface temperature of ~1250 °C was maintained for all experiments by adjusting the flame acetylene-oxygen ratio and its distance to the target. The monitor thermocouple was then removed from the impact site to the edge of the target to prevent particle deposition on its tip. The NSA surface temperature was monitored to be identical on the targets at least 10 mm up from the unsupported end. The temperature of the incoming ash particles can be considered as a function of size (spherical shape), flame-heat-transfer coefficient (heat conduction and heat capacity), and flame temperature distribution, as described by Fedosov (1976) and discussed by Taltavull et al. (2016). The correlations between distance from torch flame, grain size, and grain temperature are shown in Fig. 4. Temperature estimations from emission colors during the time of flight are consistent with these calculated temperature trends, as smaller particles of a given composition (similar crystal/glass ratio) were observed to have a more white emission color and be more rounded. The maximum flame core temperature was not measured, but is calculated to be about 3100 °C in the hot part ~10 mm away from the nozzle (Henning and Tingwaldt, 1928; Fedosov, 1976). Flames temperature distribution profile was possible to measure below 1700 °C, monitored by a S-type thermocouple. The combination of calculated and measured temperature profile along the micro-torch is shown in Fig. 4 (orange line) and is consistent with the model of Fedosov (1976), falling off faster than a large torch due to the lower gas flow rate (shorter flame).

The mean particle velocity for the size range of 160–50 μm was measured to be well above 1.5 m/s by tracking individual particles by DV images, consistent with 15 m/s from the modelling of Fedosov (1976). Melting of particles during their time of flight was indicated by changes from angular to rounded particle shape. After the ash was deposited, the flame was turned off and the deposits allowed to cool/solidify. This step simulates the cooling in an actual turbine due to shutdown either by 'flame-out' stalling or by pilots following the official 'procedure to clean the turbine blades' by 'in-flight' removal after an ash cloud encounter. The deposit was filmed for a further 5–10 min to observe any subsequent dislodgement of deposit from the blade.

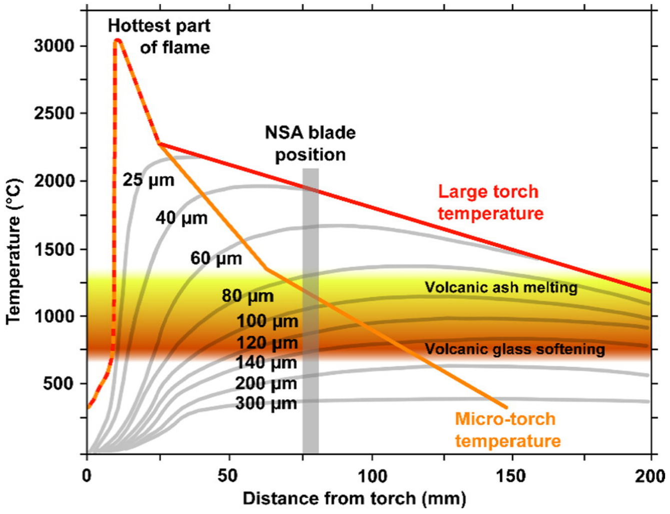

Fig. 4. Schematic illustration of the temperature distribution in an acetylene-oxygen flame. The red curve illustrates the temperature in a large torch and the grey curves show the calculated temperature of particles with respect to their size as a function of distance from the torch (from Fedosov, 1976). The red-yellow area covers the temperature range from softening point of volcanic glass (T_g) to complete melting (T_m). The orange curve is the temperature for the micro-torch used in this study (measured for the solid part). The particle size-dependent temperature curves given for the large torch would curve over to approach the orange temperature profile, the exact profiles depend on the flame-heat transfer coefficient for the different materials. However, this schematic reveals for example that 120 μm sized glass particles reach their softening point (T_g) while impacting the blade (in 6 ms), whereas particles smaller than 80 μm will be partially to completely molten (near or above T_m depending on the composition). Particles 140 μm or larger will impact as a solid.

Particle travel time in the flame is 6–30 ms (calculated for ~50 mm travel distance at ~3–15 m/s particle velocity determined by DV sequence and calculation in Fedosov, 1976). This is comparable to the 10 ms that a volcanic ash particle might typically spend in the combustion flame of a jet turbine (Kim et al., 1993), even though the particle flight distance is shorter (i.e. particle velocity is lower). Considering the experimental flight distance of 50 mm along the flame, particles <140 μm should reach >500 °C and those below 80 μm will get well above 1100 °C (Fig. 4).

This experimental setup has some important differences compared to Taltavull et al. (2016) who used a plasma torch in a vacuum chamber to fire basaltic ash on a stainless steel target 500 mm away. Their particles were calculated to travel about ten times faster than in this study, but the distance is ten times greater. So although the time of flight in the flame is similar, the greater distance means that the temperature profile drops off dramatically during flight and the target surface is not maintained at a realistic turbine temperature. The Taltavull et al. (2016) experiments provide important information related to the initial particle contact with a relatively cold metal target, but do not show the deposit build-up with time. Dean et al. (2016) used the same plasma torch set up to test a range of 'basaltic' compositions, but also used a gas gun to fire heated samples (held above their melting point) onto a metal target.

3. Results

By studying the DV recordings (eSupp. 2a–f) which are also summarised in Fig. 5, we can divide the time-resolved interaction of the incoming hot particles with the NSA target in four major categories: 1) Initial particle contact with the NSA target, 2) initial base layer build-up and on-blade heating, 3) deposit evolution during further on-blade heating and accumulation and 4) deposit behaviour (± dislodgement) upon cooling. In descriptive terms, the deposits have three main characteristics which remain after quenching; i) clear areas of melt in which 'rounded' particles fully coalesce at high temperature to form single bodies or melt pools (Figs. 5d, h and 6a); ii) porous melt, which also form rounded beads that also quench to shiny glass (sometimes with crystals visible inside), but these do not coalesce (Figs. 5t and 6b); iii) cinders which may be rounded or angular and quench to a dull appearance (Figs. 5i, p, x and 6c, d). The interaction behaviour of ash particles with the NSA blade target is initially controlled by the degree of in-flight melting and melt viscosity. The most striking feature is correlation between wetting of the blade surface and SiO_2 content, initial crystal proportion and particle size. Screenshots (Fig. 5) show the different stages (1–4) of deposit build-up and the adhesion behaviour of different ash types. Fine particles of basaltic glassy ash clearly wet the metal surface (Fig. 5a–d, see also Taltavull et al., 2016) but basalt with crystals tends to form an initial cinder layer, then build-up a melt layer on top of this (Fig. 5e–h). This is a key observation. Andesitic ash (glassy or partially crystalline) mostly stick to the blade on impact but form a cinder deposit more readily than the basaltic samples (Fig. 5m–p). Dacite and rhyolite ash particles produce hardly any surface wetting and much weaker adhesion on the blade than basalt and andesite. A higher proportion of particles bounce off upon impact. The dacite and rhyolite glasses tend to form more porous melt deposits than cindery aggregates, however a cindery contact layer was observed for dacite (Fig. 5q–t, dacitic ash, and u-x, rhyolitic ash). Quartz (not shown) represents the end-member where all particles look angular during their flight through the flame (consistent with a high melting point of 1713 °C) and bounce off the blade with no adhesion/deposition. The following more detailed description of the deposit build-up illustrate the interaction in more detail and the potential dangers for turbine failure.

Please cite this article as: Giehl, C., et al., An experimental simulation of volcanic ash deposition in gas turbines and implications for jet engine safety, Chem. Geol. (2016), http://dx.doi.org/10.1016/j.chemgeo.2016.11.024

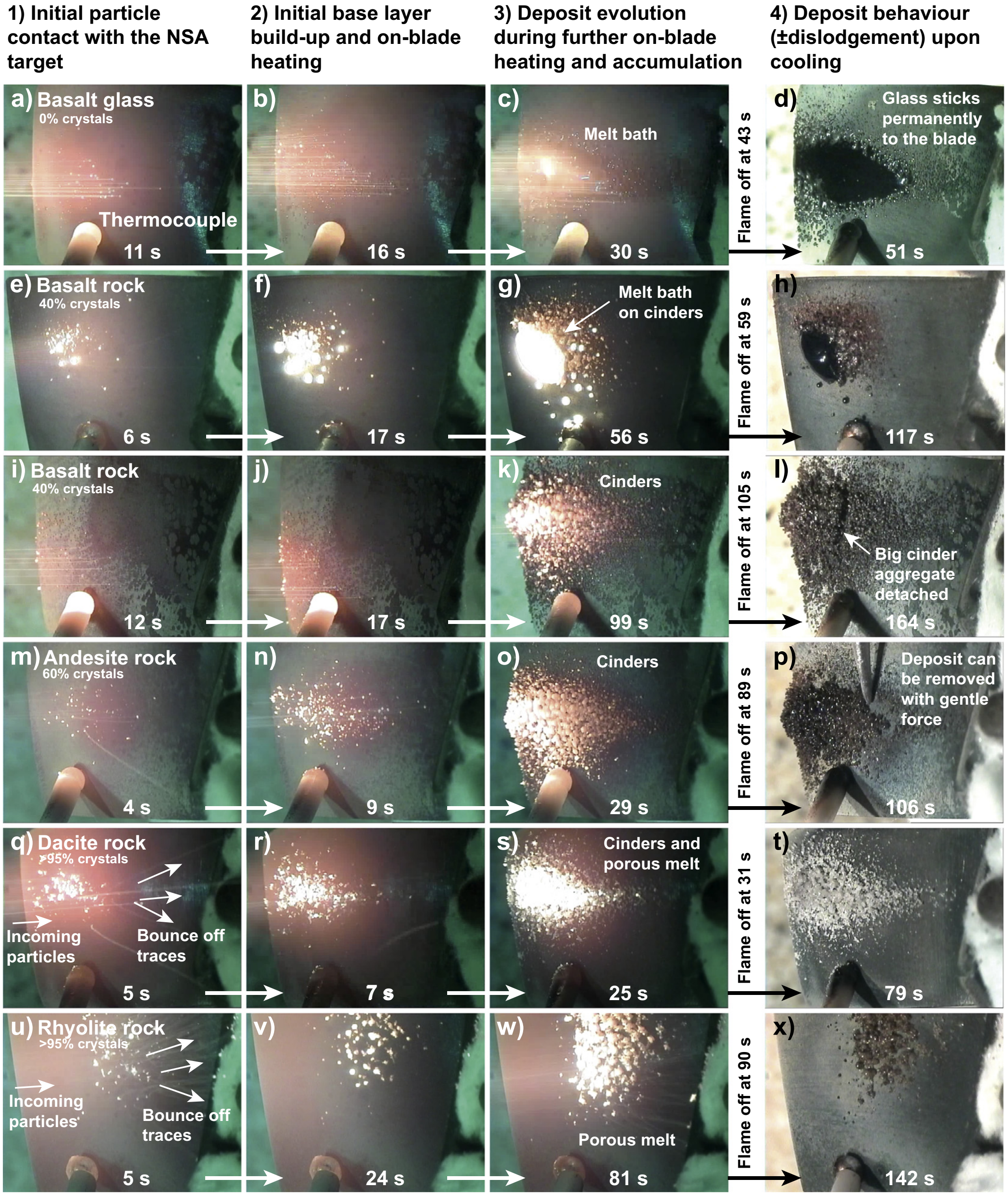

Fig. 5. Contact behaviour and development of different starting materials with time. All experiments were performed with a grain size fraction of 125–5 μm. The first three photographs of each line are taken with the flame on and the blade at 1250 °C. The last photograph of each line is taken after cooling, where the material is solid. (a)–(d) illustrates basalt glass 'ash' with the deposit wetting the surface to form a melt bath. (e)–(h) is basalt rock, first forming a cinder layer, with subsequent particles showing on-blade melting to form a melt bath on top. (i)–(l) is also a basaltic rock where porous melt forms during continuous heating, a big cinder aggregate falls off after cooling at 150 °C. (m)–(p) is an andesite rock, early hot particles bounce off the blade before a cinder deposit starts to form during continuous heating. The deposit remains after the flame is turned off, but can be easily removed. (q)–(t) is a dacite rock showing particles bouncing off and later formation of cinders and porous melt. (u)–(s) is a rhyolite rock also showing bouncing off particles and porous melt formation. Note detached deposits in (x) after cooling compared to (w). Width of blade is 10 mm. The timeline starts (0 s) when the first particle hits the blade. All photographs are screenshots from DV that can be found in the electronic supplement (eSupp. 2a–f).

3.1. Initial particle contact with the NSA target

The videos (eSupp. 2a–f) illustrate that particles in the flame are well-heated, usually showing yellow to white emission colors (Fig. 5a). However, for this experimental set up, there is a 'critical' maximum particle size for a deposit to form of around 300 μm, larger particles generally bounce off regardless of composition (Fig. 5u, eSupp. 2a). This may reflect insufficient heat transfer in the flame for their given mass (Fig. 4) and a lack of melting, although some smaller fully molten (rounded) particles also bounce off (see Discussion, Section 4.2). Particle size also controls the degree of wetting when hitting the NSA blade. Glass and crushed rock powders with smaller grain sizes stick to the blade as well-rounded (mostly molten) or more commonly partly rounded/angular cinder particles (partly molten at the rim). Particles with higher SiO_2 contents tend to remain more rounded on the blades' surface (also shown in Fig. 6b). However, for the lower SiO_2 compositions, the smallest fully molten impacting particles tend to spread out on contact to form splats (see Fig. 6a) and start to efficiently wet the target surface. This phenomenon (also observed by Taltavull et al., 2016) has important consequences as further incoming particles accumulate as melt on these initial splats. The larger impacting basalt particles tend to form larger rounded spheres (Fig. 6c) with higher wetting angles (eSupp. 3d).

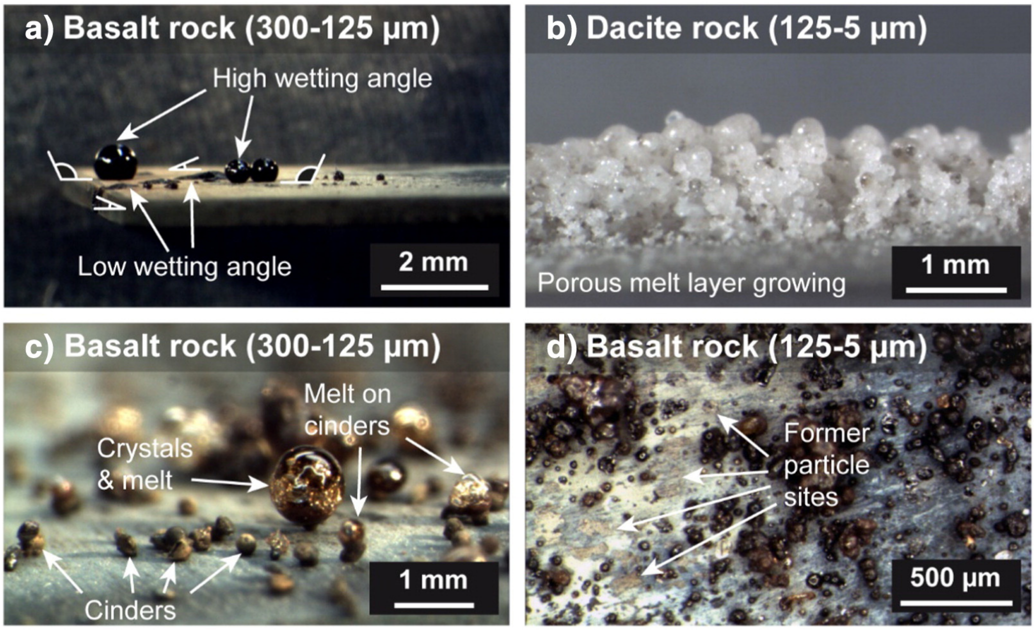

Fig. 6. Wetting features on NSA blade deposits after cooling to room temperature. (a) The basalt rock displays wetting of smaller particles, but less wetting for larger particles that arrived with less heating. In (b) the melt (dacite rock) forms a porous melt layer with up to 2 mm height. (c) is basalt rock, with incoming particle sizes too big to melt completely during flight in flame. First particles form cinder, but during further deposition, melt spheres grow on top of the cinders, perhaps insulated from the blade (note they are bigger than the incoming ash). In one sphere, glass (dark/brown) and crystals (shiny/clear) can be seen. These spheres never form directly on the metal surface. In (d) the basalt rock particles partly detached during and after cooling. Here, detached particles also remove a layer from the NSA surface to expose fresh metal.

3.2. Initial base layer build-up and on-blade heating

Particles on the blade remain in the flame at ~1250 °C and on-blade heating can maintain or produce further melting, so it is possible that initial angular particles sticking to the blade surface become rounded. However, it is more common that the cinder contact layer remains unchanged and molten material accumulates on top (Fig. 5e, k, o, s). This is clearly illustrated in Fig. 6c where large molten spheres grow on top of smaller cinder particles. This on-blade melting enhances the consolidation of aggregates and allows extensive acceleration of aggregate accumulation, particularly for basalt rock.

Despite a lower liquidus temperature, the more SiO_2-rich ashes appear to show a lower degree of on-blade melting and retain some particles that are dominantly angular and cinder like. Their aggregates are only weakly attached to the blade itself ('cinders', see Fig. 6c). The build-up of melt above a cindery layer is one of the most common observations in this study. There are a few cases where there appears to be a very thin melt layer perhaps formed by the initial smallest particles (see 'low wetting angle' in Fig. 6a) with a cindery aggregate on top. Also, the finer incoming particles can fill the space between cinders. These both tend to help the coating adhere more coherently to the blade.

3.3. Deposit evolution during further on-blade heating and accumulation

In general, deposit formation during continuous heating is characterized by filling the space between particles. Cindery particles are usually bigger and more rounded than the initial starting material and can 'grow' and then sinter together with time (see also Song et al., 2014). The original cinder shape is maintained unless the spacing between is filled with new particles (Fig. 5k, eSupp. 2b). Cinder layer build-up is most common when a partially crystalline crushed rock is used as starting material and is mainly a consequence of melting being confined to the outer surface of the minerals which require significant enthalpy to melt compared to the glass. Samples of the cooled deposits often show a glass coating on the surface of minerals. This glass coating is also a common feature of minerals in our crushed rocks, so it is not easy to distinguish if this feature is pre-existing or related to in-flight partial mineral melting. In both cases, high-temperature layer accumulation/adhesion is possibly related to the presence of this melt layer. In some cases, these cindery deposits can also include angular particles of glass that attach to the blade and melt very slowly.

Incoming particles captured on top of cindery deposits can start to melt, accumulate more particles and form either a ponded melt bath in the case of basalt and andesite (Fig. 5h) or a 'porous melt layer' for the SiO_2-rich compositions. This porosity is due to the space left between the individual, un- or semi-coalesced, rounded growing spheres (Figs. 5t and 6b) with may also retain some crystals (eSupp. 3a). This porosity may be enhanced by degassing of dissolved volatiles into the pores. After cooling, the glassy 'spheres' remain stuck together, as commonly observed for dacite rock (Fig. 6b, eSupp. 3b). This is more typical for SiO_2-rich compositions (dacite and rhyolite) reflecting their higher melt viscosities to some extent. There can be a mixture of porous melt and cinders in a deposit (Fig. 5s, eSupp. 2e).

3.4. Deposit behaviour (±dislodgement) upon cooling

Cinders tend to be irregular shaped particles that usually have a dull appearance when cooled to room temperature (Fig. 6c). They play an important role when the deposit is cooled. Individual particles as well as quenched melt droplets on top of the cinder deposit start to jump off the blade as they cool below 500–100 °C. In all cases where an initial cinder layer is next to the blade, the deposits detach and fall off on cooling to room temperature within 3–4 min or can be removed with gentle force (Fig. 5p, eSupp. 2d).

In Fig. 6c, angular particles can be seen sticking to a sphere before being melted and/or being adsorbed into the growing melt. In some cases, minerals can be seen inside these spheres (Fig. 6c). However, it is more common that the angular particles stick to other non-melted (cindery) material rather than the blade itself. This material falls off the blade on cooling as there is no real wetting of the metal, although this can change if there is some chemical reaction (Fig. 6d, eSupp. 3e).

Please cite this article as: Giehl, C., et al., An experimental simulation of volcanic ash deposition in gas turbines and implications for jet engine safety, Chem. Geol. (2016), http://dx.doi.org/10.1016/j.chemgeo.2016.11.024

There can be a thin, irregular glassy deposit remaining on the blade that indicates some reaction with the NSA and the detached particles or fresh metal indicating the reacted surface has gone (Fig. 6d). In strong contrast, small splat melts (Fig. 6a) and ponded melts (Fig. 5d) remain unchanged during cooling and do not detach from the blade even if considerable force is used (eSupp. 3c–e).

4. Discussion

4.1. Size is important

Due to efficient particle size reduction in the compressor (Clarkson et al., 2016), it is possible that the ash entering a combustor is milled to a size fraction at the lower end of the range tested in this study. The larger particles may not be relevant to actual jet engine encounters, but remain useful to simulate some features of particle melting kinetics within our experimental setup. The theoretical effect of heat transfer to different particle sizes as illustrated in Fig. 4, suggests that any grain smaller than 60 μm will reach the temperature of the combustor flame, even up to 1500 °C. If all ash entering the turbine after being milled in the compressor is 6 μm (Clarkson et al., 2016), all glass and all minerals in volcanic ash might be expected to melt 100%. A compilation of 50 experimental runs are presented in Fig. 7 and along with the summary observations presented in Fig. 5, generally support the schematic temperature-grain size relationship in Fig. 4. Large grain sizes, 500 to 125 μm, are more likely to bounce off the blade and thus barely form any deposit. We only present selected reliable data on specific particle sizes smaller than 63 μm due to high bulk compositional variation in this sieved fraction, but for mixtures with grain sizes of 125–5 μm, the results are consistent with a high level of melting. As described previously, any melt formed on the blade by smaller particles, will ‘capture’ larger particles and allow them to melt. Hence, the smaller fraction in the ash takes on an important role. Our 125–5 μm ash mixtures are probably the most realistic starting materials with respect to real ‘in-flight’ encounters so it is no surprise that our textures reflect those observed in damaged engines (see below).

4.2. The characteristics of experimental and natural ash deposits

The changes in the deposit with time are best viewed in the videos (eSupp. 2a–f) but are also shown in Fig. 5. As noted above, the nature of the initial deposit is important as it controls the subsequent accumulation of material. While the angle of incidence and the condition of the metal surface appear to have some secondary influence on whether molten particles bounce off or not (Taltavull et al., 2016), the most significant parameter in this study appears to be the bulk visco-elastic response of the molten particle (see also Senior and Srinivasachar, 1995). This correlation is easiest to observe for particles that are clearly 100% molten (or above T_g). It is not easy to identify partially molten particles in our experiments but the DV recording clearly show that more angular particles do tend to bounce off the blade more often, as might be expected if they have a ‘solid’ core. However, some particles that are clearly 100% melts also bounce off with surprising regularity. This is more common for melts with higher SiO_2 contents, but is also observed for smaller particles with lower SiO_2 (predicted to be 100% melt). This behaviour might be related to the ‘fragility’ of the liquid (Toplis et al., 1997) where it acts as a solid at the high strain rate experienced during impact.

Cindery particles are interpreted as partially molten and ‘coated’ with melt allowing them to stick to the blade. The nature of the deposit can change with time and accumulation. In our experiments, deposits develop in one of three ways:

i) continuing accumulation as cinders on top of a cindery initial deposit (Fig. 5u–w)
ii) the development of a pool of melt (a glaze) or a porous melt on top of the cinder deposit (Fig. 5i–k, m–o, q–s)
iii) the continued accumulation of splat melt to form a melt bath (a term borrowed from welding terminology, Fig. 5a–c)

If the deposit starts as a cindery (or porous melt) layer this feature appears to insulate further incoming particles from conductive cooling effects of the blade. It is important to remember that the particles spend a short time (milliseconds) travelling in the flame as they transverse the combustor, but this is followed by a much longer period (minutes) sitting on the blade, albeit in a cooler part of the flame (1250 °C in these experiments but could be even higher in modern engines). In the case of air cooled blades and the experimental simulations here, the metal surface is continually conducting heat away with a thermal gradient of > 500 °C/mm to giving a measured temperature of < 1000 °C at the back of the experimental blade. The ‘insulating’ behaviour of cindery

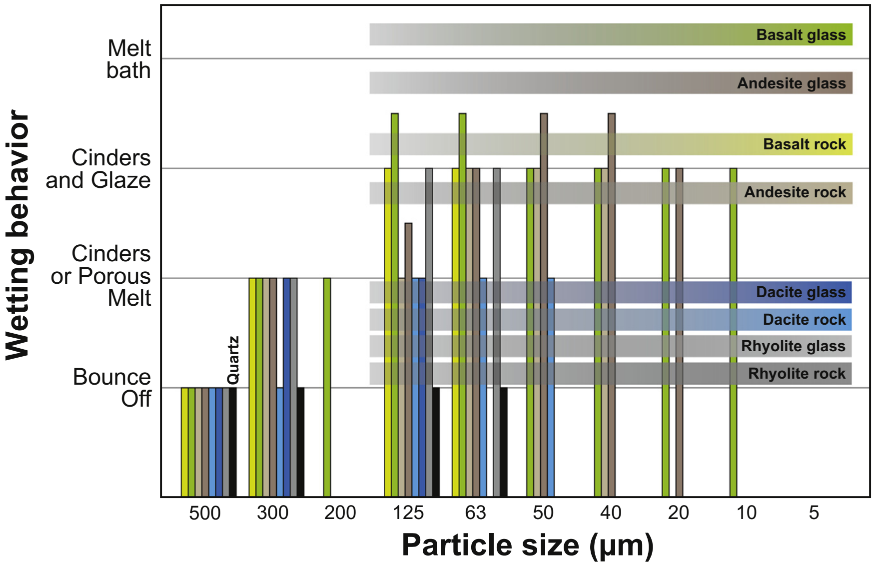

Fig. 7. Behaviour of different ash compositions and quartz with respect to particle size. ‘Bounce off’ is rare for compositions/sizes that also stick to the blade, but is observed at early stages on a clean NSA target. The range of behaviours represents initial contact behaviour and deposit evolution and accumulation with time. The smaller particles in the mixed 125–5 μm fraction are possibly the most important controlling factor for build-up of deposits.

material is clearly demonstrated in Fig. 6c, where many of the cinders have melt spheres growing on top. Mixtures of cinders and porous melt in one experiment can also derive from different grain sizes and melt proportion of particles. The cindery or porous substrate allows further accumulation particles to reach the temperature of the flame next to the blade at 1250 °C, which is above T_m for most volcanic ash compositions. This facilitates an increase in the accumulation rate of the material adhering to the deposit, rather than bouncing off, and particles can melt completely to form a molten pool (melt bath) or 'glaze' on the cinder layer. 100% glassed starting materials are favoured for this 'on-blade' process, as a bigger range of grain size have time to reach the flame temperature. In general, the presence of any small amounts of melt will move the system away from the individual controls of glass softening (T_g) and mineral melting (T_m), but towards the lower temperature eutectic melting control of the bulk rock composition. For the minerals in our study (mainly olivine and plagioclase), it is unlikely that they will melt on the blade in the 1250 °C flame as individual ash particles, but eutectic melting is possible. There is also evidence that molten particles at the interface to the blade can react with the NSA blade as shown in Fig. 6d. This confirms that even if ash particles detach after some time sticking to the turbine blade, corrosion might be an issue, as was also observed during a NASA research flight during the Mt Hekla eruption (Grindle and Burcham, 2003, Fig. 8b). After detachment of the cindery deposit during cooling, a thin, irregular glassy deposit can be left on the blade. This irregular glaze is probably formed due to some chemical reaction with the metal. Cinder deposits with 'molten tops' were observed in the studies summarized by Kim et al. (1993) when using Blend 2 and black scoria compositions where they describe 'grainy' agglomerations next to the air-cooled vanes covered by a 'glaze-like' coating, all of which were very easily removed after the experiment. This texture is also present in the turbine engine of the 1982 Mt Galunggung encounter as shown in Fig. 8a.

eSupp. 3c and d show the contact of a quenched melt bath (basalt) on the NSA target. There are cracks within the glass parallel to the interface and it remains unclear if these are related to thermal shock when the flame is turned off or during sample preparation. Dendritic crystals observed in the glass at the interface to the NSA blade (eSupp. 3e) can be interpreted as quench crystals that formed during impact and/or cooling on the target to well below 1250 °C (below the liquidus of around 1100 °C). Where melt splats form the initial deposit, it was observed that some of these 'retreated' on the NSA surface to form more spherical blobs with a higher wetting angle. The splat melt feature is probably due to flattening on impact (low viscosity) and efficient quenching below T_g on the 'cool' blade. If temperature of the 'on-blade' particle can subsequently be heated above T_g, the splat can reform towards higher wetting angles similar to static experiments (not presented here). The much higher impact speed and colder target temperature in the basaltic experiments of Taltavull et al. (2016) and Dean et al. (2016) generally result in the formation of 'quench splats' which have little chance of reheating in the thermal regime of those particular experiments. It should be noted that 3 to 5 times more material was fired at the target in this study compared to Taltavull et al. (2016) and Dean et al. (2016) so there is more chance for a deposit to develop. However, it is clear that the percentage of adhered material for a comparable basaltic composition is considerably higher in this study approaching 80–100% with the blade at 45°. This compares with 5–20% with a 30° blade and 10–35% for a blade at 60° in the 'cooler' Taltavull et al. (2016) experiments.

4.3. Application and scaling to real jet turbine engines

Given the large range of engine designs and in particular temperature regimes, it is difficult to directly apply our results to modern turbines. However, our acetylene-oxygen flame temperature (Fig. 4) covers a range from higher to lower temperatures compared with a jet engine combustor (Fig. 1b). Our deposited ash temperature of ~1250 °C just above the blade surface and <1000 °C at the back, is probably a realistic representation of temperatures during normal flight, although not maximum thrust during a climb. We do not simulate the thin-air-film cooling used in modern blade designs, but in any case particles would hit the blade with high temperatures unless deflected by the flowing air film. Also, the air supplied to cool the vanes and turbines is tapped from the compressor, so is already heated due to compression (to ~625 °C, Fig. 1b) before it is heated further during heat exchange. However, the thin layer of the cooling air enveloping the vanes and blades in modern engines makes this complicated interface difficult to assess. At higher experiment temperatures and thus shorter torch-target distance, NSA blades would melt and particles would heat up less due to shorter travel time within the flame. This may or may not be the case for the particle speeds reached in a modern turbofan and therefore needs further consideration. It should be noted that the carefully designed aerodynamically controlled thin-air-film layer will rapidly become unstable if any deposits are formed on the surface or even some of the holes supplying the cooling air are blocked by either molten or any solid particles. Dunn (2012) reported such a blockage of the cooling system and the resulting melting of turbine blades.

Our observed transition from cinders to melt due to thermal insulation has also been observed in pulverised coal burning furnace of power plants where silicate and sulphide impurities present in the coal stick to the tubes used to exchange heat to the water. At first the sulphur is involved in forming molten coatings to make silicate ash particles sticky, resulting in a porous cinder layer (Walsh et al., 1990). This process increases the surface temperature and the silicate ash starts to accumulate as a molten layer above the porous deposit (e.g. Richards et al., 1993). A similar phenomenon also occurs during firing of coal in entrained-flow gasifiers (Song et al., 2009, 2011). On the interior wall of such gasifiers, liquid slags form on top of solid slags. In our study, the system is at higher temperatures and the 'heat exchanger' is the NSA blade cooled by a thermal gradient rather than the more efficient flow of water steam in a boiler.

In the past, this cinder layer proved critical to the planes caught in ash clouds and there are similarities between some of experimental

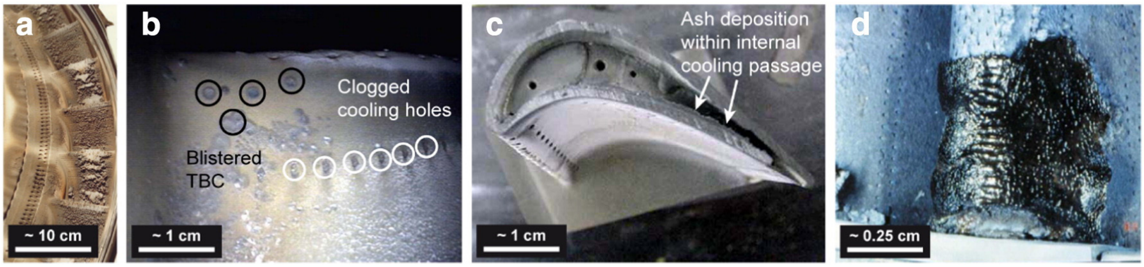

Fig. 8. (a) Cindery deposit and melt glaze on turbine vanes (this is the support, not the moving blade part) from the recovered British Airways 747 engine that stalled in the ash cloud of the 1982 basaltic eruption of Mt Galunggung, Indonesia (courtesy Eric Moody). (b) and (c) are coated blades from a NASA research airplane that purposely flew through a diffusive volcanic ash cloud of Mt Hekla in 2000 (courtesy Thomas J. Grindle). (d) is a melt bath on a damaged blade from the Boeing 747 that flew through the 1989 Redoubt ash cloud. Part of damage costing US $ 80 million to repair (courtesy USGS).

deposits and engines recovered from ash encounters. Fig. 8a shows the actual deposits in the turbine of an engine that stalled in an ash encounter (1982 basaltic eruption of Mt Galunggung, Indonesia) with similarities to the basaltic ash deposit produced in our experiments. Both have the same cindery appearance and the real turbine also has an 'on-blade' melting glaze on top of the cinders (compare with Fig. 5g, h). The cindery deposit on the experimental blade detached during cooling, as was the case for the Mt Galunggung encounter which allowed two of the four engines to be restarted 'in-flight'. This has become the 'standard procedure', to allow the engine to cool and hope the ash deposit is dislodged, and then restart the engine. The difference between the cindery or cinder 'insulated' deposits in Fig. 5e–h and the 'wetted surface' melt bath in Fig. 5a–d is clearly a cause for concern. Such a 'wetted surface' in an actual turbine is illustrated in Fig. 8d (compare to Fig. 5d), showing a damaged blade exposed to ash from the 1989 andesitic Redoubt eruption. The melt bath will not dislodge by any means as it quenches to a glass after the engine stalls or is shut down. Luckily in this case the engines were successfully restarted 'in-flight' after losing 7500 m altitude even though the blade had started to melt.

Detachment of cindery particles may also have some detrimental effect in modern engines as they might stick to and carry away parts of TBC's. Delamination of TBC's can be due to wear (e.g. Bumgardner and Li, 2015), but material loss of the NSA blade was also documented in some of our experiments where cindery particles carry parts of the NSA (Fig. 6d). Any dislodging particles can also clog cooling holes and cooling channels as seen on Fig. 8b and c (taken from Grindle and Burcham, 2003).

Newly developed CMC materials (mainly composed of silicon carbide) are lightweight alternative to NSA and have a significantly higher T_m. During normal operation, TBC's are expected to protect CMC blades, but damage to the TBC's will also result in high vulnerability of new turbine engines when exposed to volcanic ash. However, a recent study by Crazzolara (2015) shows that silicon carbide is highly reactive when exposed to silicate melt using similar melt compositions to this study. Possible modifications of turbine design to decrease vulnerability to volcanic ash are possible (Davison and Rutke, 2014), but unlikely due to higher operational cost and the infrequency of encounters. The 2010 Rolls Royce 'safe-to-fly' chart (see Davison and Rutke, 2014; Clarkson et al., 2016) and an ash cloud concentration limit of 2 mg/m^3 is clearly a useful 'rule of thumb' but as suggested by Nowak et al. (2011, 2013), Dunn (2012), Taltavull et al. (2016) and clearly illustrated in this study, the composition and crystal/glass ratio of the ash has a significant bearing on the acceptable ash limit. Perhaps a small sensor that emulates the exact 'in-flight' engine conditions could be developed for aircraft which is very sensitive to the adhesion properties of heated ash at an early stage of any ash cloud encounter.

5. Conclusions

As illustrated by these experiments, the chemical composition and crystal/glass ratio exert strong controls on the way deposits form on turbine blades. As a result, these ash characteristics should also be considered when setting safety limits for ash concentration in airspace. Previous standard tests (Arizona Road Dust) are certainly not realistic and do not address the true extent of the risks involved. Our dynamic experiments illustrate how the range of volcanic ash compositions and crystallinities commonly found in nature can have different effects on both the build-up and the possible 'in-flight' removal of the deposits. Policy makers and industry should consider advice from the geological community regarding volcanic ash encounters and rapidly analyze the petrological nature of ash as well as the particle size distribution. Further interaction experiments are undoubtedly required, especially considering the recent development of new turbine materials.

Supplementary data to this article can be found online at http://dx.doi.org/10.1016/j.chemgeo.2016.11.024.

Acknowledgements

Our thanks go to Norbert Walker and Daniel Russ for technical support and advice. We further acknowledge two anonymous reviewers and Oliver Beermann for constructive comments that helped to improve the manuscript. Sincere thanks are given to Eric Moody and Thomas J. Grindle for their permission to use turbine blade photographs. We also thank Rory Clarkson for encouraging us to finally publish these data as we enter a new period of 'glasnost' with the airline industry. This study was financed by overheads of grant NO 378/5-1 of the German Science Foundation (DFG).

References

Brooker, P., 2010. Fear in a handful of dust: aviation and the Icelandic volcano. Significance 7:112–115. http://dx.doi.org/10.1111/j.1740-9713.2010.00436.x.

Brun, K., Nored, M., Kurz, R., 2012. Particle transport analysis of sand ingestion in gas turbine engines. J. Eng. Gas Turbines Power 134:012402. http://dx.doi.org/10.1115/1.4004187.

Budd, L., Griggs, S., Howarth, D., Ison, S., 2011. A fiasco of volcanic proportions? Eyjafjallajökull and the closure of European airspace. Mobilities 6:31–40. http://dx.doi.org/10.1080/17450101.2011.532650.

Bumgardner, C., Li, X., 2015. Unveiling Ultra-High Temperature Wear and Indentation Damage Mechanisms of Thermal Barrier Coatings. J. Miner. Met. Mater. Soc. 67 (12):2921–2933. http://dx.doi.org/10.1007/s11837-015-1622-2.

Bursik, M.I., Sparks, R.S.J., Carey, S.N., Gilbert, J.S., 1991. The Concentration of Ash in Volcanic Plumes, Inferred from Dispersal Data. 1st International Symposium on Volcanic Ash and Aviation Safety, Seattle, WA, July 8–12. United States Geological Survey, Washington, DC, pp. 19–29.

Campbell, E.E., 1990. Volcanic Ash. Proceedings of the 747 Flight Operations, Symposium, Seattle, WA, 9.-11.10.1990. Boeing Commercial Aircraft Company, pp. 2.3.1–2.3.34.

Casadevall, T.J., 1994. The 1989–1990 eruption of Redoubt Volcano, Alaska: impacts on aircraft operations. J. Volcanol. Geotherm. Res. 62:301–316. http://dx.doi.org/10.1016/0377-0273(94)90038-8.

Casadevall, T.J., Delos Reyes, P.J., Schneider, D.J., 1999. The 1991 Pinatubo Eruptions and Their Effects on Aircraft Operations. University of Washington Press, U.S.·Geological Survey (URL: pubs.usgs.gov/pinatubo/casa/).

Chambers, J.C., 1985. The 1982 Encounter of British Airways 747 with the Mt. Galunggung Eruption Cloud. AIAA paper 85-0097, AIAA 23rd Aerospace Sciences Meetings, 14.-17.1.1985, Reno, Nevada.

Christmann, C., Nunes, R.R., Schmitt, A.R., 2015. Recent Encounters of Aircraft with Volcanic Ash Clouds. Deutscher Luft- und Raumfahrtkongress (2015 Document ID: 370124).

Cioni, R., Pistolesi, W., Bertagnini, A., Bonadonna, C., Hoskuldsson, A., Scateni, B., 2014. Insights into the dynamics and evolution of the 2010 Eyjafjallajökull summit eruption (Iceland) provided by volcanic ash textures. Earth Planet. Sci. Lett. 394:111–123. http://dx.doi.org/10.1016/j.epsl.2014.02.051.

Clarkson, R.J., Majewicz, E.J.E., Mack, P., 2016. A re-evaluation of the 2010 quantitative understanding of the effects volcanic ash has on gas turbine engines. Proc. Inst. Mech. Eng. G J. Aerosp. Eng. 230:2274–2291. http://dx.doi.org/10.1177/0954410015623372.

Crazzolara, C., 2015. Untersuchungen zur Gasentwicklung von Silikatschmelzen bei Temperaturen um 1.200 °C und einem Druck von 1 bar in Anwesenheit von Siliciumcarbid. B.Sc. Thesis. University of Tübingen (82 pp).

Davison, C.R., Rutke, T.A., 2014. Assessment and characterization of volcanic ash threat to gas turbine engine performance. J. Eng. Gas Turbines Power 136:081201. http://dx.doi.org/10.1115/1.4026810.

Dean, J., Taltavull, C., Clyne, T.W., 2016. Influence of the composition and viscosity of volcanic ashes on their adhesion within gas turbine aeroengines. Acta Mater. 109:8–16. http://dx.doi.org/10.1016/j.actamat.2016.02.011.

Drexler, J.M., Gledhill, A.D., Shinoda, K., Vasiliev, A.L., Reddy, K.M., Sampath, S., Padture, N.P., 2011. Jet engine coatings for resisting volcanic ash damage. Adv. Mater. 23: 2419–2424. http://dx.doi.org/10.1002/adma.201004783.

Dunn, M.G., 2012. Operation of gas turbine engines in an environment contaminated with volcanic ash. J. Turbomach. 134:051001. http://dx.doi.org/10.1115/1.4006236.

Dunn, M.G., Baran, A.J., Miatech, J., 1996. Operation of gas turbine engines in volcanic ash clouds. J. Eng. Gas Turbines Power 118:724–731. http://dx.doi.org/10.1115/1.2816987.

Fedosov, V.V., 1976. Particle temperature in the gas flame during powder fusion cladding. Chem. Pet. Eng. 12:259–262. http://dx.doi.org/10.1007/BF01145853.

Giehl, C., Brooker, R.A., Marxer, H., Nowak, M., 2016. The Effect of Volcanic Ash Composition and Glass Content on Jet Engine Safety. European Mineralogical Conference, Rimini, Italy (09/2016).

Giordano, D., Russell, J.K., Dingwell, D.B., 2008. Viscosity of magmatic liquids: A model. Earth Planet. Sci. Lett. 271:123–134. http://dx.doi.org/10.1016/j.epsl.2008.03.038.

Gislason, S.R., Hassenkam, T., Nedel, S., Bovet, N., Eiriksdottir, E.S., Alfredsson, H.A., Hem, C.P., Balogh, Z.I., Dideriksen, K., Oskarsson, N., Sigfusson, B., Larsen, G., Stipp, S.L.S., 2011. Characterization of Eyjafjallajökull volcanic ash particles and a protocol for rapid risk assessment. Proc. Natl. Acad. Sci. 108:7307–7312. http://dx.doi.org/10.1073/pnas.1015053108.

Grindle, T.J., Burcham, F.W., 2003. Engine Damage to a NASA DC-8-72 Airplane from a High-altitude Encounter with a Diffuse Volcanic Ash Cloud. Technical Memorandum, 22 pp. NASA, Edwards, California, USA (NASA/TM-2003-212030 2003. URL: alpa.org/portals/alpa/volcanicash/03_NASADC8AshDamage.pdf).

Guffanti, M., 2004. Reducing Encounters of Aircraft with Volcanic-Ash Clouds. Proceedings of the 2nd International Conference on Volcanic Ash and Aviation Safety. Office of the Federal Coordinator for Meteorological Services and Supporting Research: pp. 17–21 session 1. (URL: ofcm.gov/ICVAAS/Proceedings2004/pdf/10-session1.pdf).

Guffanti, M., Casadevall, T.J., Budding, K., 2010. Encounters of Aircraft with Volcanic Ash Clouds: A Compilation of Known Incidents. U.S. Geological Survey, pp. 1953–2009 (Data Series 545. URL: pubs.usgs.gov/ds/545/).

Hanstrum, B.N., Watson, A.S., 1983. A case study of two eruptions of Mount Galunggung and an investigation of volcanic eruption cloud characteristics using remote sensing techniques. Aust. Meteorol. Mag. 31, 171–177 (URL: bom.gov.au/amm/docs/1983/hanstrum.pdf).

Harmon, R.S., Gerbe, M.C., 1992. The 1982–83 eruption at Galunggung Volcano, Java (Indonesia): oxygen isotope geochemistry of a chemically zoned magma chamber. J. Petrol. 33:585–609. http://dx.doi.org/10.1093/petrology/33.3.585.

Henning, F., Tingwaldt, C., 1928. Die Temperatur der Acetylen-Sauerstoffflamme. Z. Phys. 48:805–823. http://dx.doi.org/10.1007/BF01331994.

IATA Economic Briefing, 2010. The Impact of Eyjafjallajökull Volcanic Ash Plume. International Air Transport Association (URL: iata.org/whatwedo/Documents/economics/Volcanic-Ash-Plume-May2010.pdf).

Johnson, R.W., Jaques, A.L., Hickey, R.L., CO, M.K., Chappell, B.W., 1985. Manam Island, Papua New Guinea: petrology and geochemistry of a low-TiO_2 basaltic island-arc volcano. J. Petrol. 26:283–323. http://dx.doi.org/10.1093/petrology/26.2.283.

Kim, J., Dunn, M.G., Baran, A.J., Wade, D.P., Tremba, E.L., 1993. Deposition of volcanic materials in the hot sections of two gas turbine engines. J. Eng. Gas Turbines Power 115: 641–651. http://dx.doi.org/10.1115/1.2906754.

Koff, B.L., 2004. Gas turbine technology evolution: a designers perspective. J. Propuls. Power 20:577–595. http://dx.doi.org/10.2514/1.4361.

Krämer, S., Yang, J., Levi, C.G., Johnson, C.A., 2006. Thermochemical interaction of thermal barrier coatings with molten CaO–MgO–Al_2O_3–SiO_2 (CMAS) deposits. J. Am. Ceram. Soc. 89:3167–3175. http://dx.doi.org/10.1111/j.1551-2916.2006.01209.x.

Kueppers, U., Cimarelli, C., Hess, K.-U., Taddeucci, J., Wadsworth, F.B., Dingwell, D.B., 2014. The thermal stability of Eyjafjallajökull ash versus turbine ingestion test sands. J. Appl. Volcanol. 3:4. http://dx.doi.org/10.1186/2191-5040-3-4.

Kushendratno, P.J.S., Kristianto, F.R.B., McCausland, W., Carn, S., Haerani, N., Griswold, J., Keeler, R., 2012. Recent explosive eruptions and volcano hazards at Soputan volcano—a basalt stratovolcano in north Sulawesi, Indonesia. Bull. Volcanol. 74: 1581–1609. http://dx.doi.org/10.1007/s00445-012-0620-2.

Le Bas, M.J., Streckeisen, A.L., 1991. The IUGS systematics of igneous rocks. J. Geol. Soc. 148:825–833. http://dx.doi.org/10.1144/gsjgs.148.5.0825.

Mechnich, P., Braue, W., Schulz, U., 2011. High-temperature corrosion of EB-PVD yttria partially stabilized zirconia thermal barrier coatings with an artificial volcanic ash overlay. J. Am. Ceram. Soc. 94:925–931. http://dx.doi.org/10.1111/j.1551-2916.2010.04166.x.

Nowak, M., Giehl, C., Marxer, H., Brooker, R., 2011. Volcanic Ash in Jet Turbine Engines. 9th Silicate Melt Workshop. La Petite Pierre, France (10/2011).

Nowak, M., Giehl, C., Marxer, M., Brooker, R., 2013. The Impact of Volcanic Ash in Jet Turbine Engines. Geofluids, Tübingen, Germany (09/2013).

Olafsdottir, R., Sigmundsson, F., 2001. The Nordic Volcanological Institute, Reykjavik, Iceland (URL: norvol.hi.is/hekla.html).

Padture, N.P., Gell, M., Jordan, E.H., 2002. Thermal barrier coatings for gas-turbine engine applications. Science 296:280–284. http://dx.doi.org/10.1126/science.1068609.

Pieri, D., Ma, C., Simpson, J.J., Hufford, G., Grindle, T., Grove, C., 2002. Analyses of in-situ airborne volcanic ash from the February 2000 eruption of Hekla volcano, Iceland. Geophys. Res. Lett. 29:19-1–19-3. http://dx.doi.org/10.1029/2001GL013688.

Przedpelski, Z.J., Casadevall, T.J., 1994. Impact of Volcanic Ash from 15 December 1989 Redoubt Volcano Eruption on GE CF6-80C2 Turbofan Engines. 2047. U.S. Geological Service Bulletin, pp. 129–135 (URL: dggs.alaska.gov/pubs/id/4415).

Richards, G.H., Slater, P.N., Harb, J.N., 1993. Simulation of ash deposit growth in a pulverized coal-fired pilot scale reactor. Energy Fuel 7:774–781. http://dx.doi.org/10.1021/ef00042a012.

Rolls-Royce, 1996. The Jet Engine. fifth ed. (Derby, England. 278 pp, ISBN 0-902121-2-35).

Schmidt, M.E., Grunder, A.L., 2009. The evolution of North Sister: a volcano shaped by extension and ice in the central Oregon Cascade Arc. Geol. Soc. Am. Bull. 121:643–662. http://dx.doi.org/10.1130/B26442.1.

Senior, C.L., Srinivasachar, S., 1995. Viscosity of ash particles in combustion systems for prediction of particle sticking. Energy Fuel 9:277–283. http://dx.doi.org/10.1021/ef00050a010.

Sigmarsson, O., Vlastelic, I., Andreasen, R., Bindeman, I., Devidal, J.-L., Moune, S., Keiding, J.K., Larsen, G., Höskuldsson, A., Thordarson, T., 2011. Remobilization of silicic intrusion by mafic magmas during the 2010 Eyjafjallajökull eruption. Solid Earth 2: 271–281. http://dx.doi.org/10.5194/se-2-271-2011.

Smialek, J.L., Archer, F.A., Garlick, R.G., 1994. Turbine airfoil degradation in the Persian Gulf War. JOM 46:39–41 Corrosion and Erosion Research Summary. http://dx.doi.org/10.1007/BF03222663.

Song, W., Tang, L., Zhu, X.D., Wu, Y.Q., Wu, Y., Rong, Y.Q., Zhu, Z.B., Koyama, S., 2009. Fusibility and flow properties of coal ash and slag. Fuel 88:297–304. http://dx.doi.org/10.1016/j.fuel.2008.09.015.

Song, W., Sun, Y., Wu, Y., Zhu, Z.B., Koyama, S., 2011. Measurement and simulation of flow properties of coal ash slag in coal gasification. AICHE J. 57:801–818. http://dx.doi.org/10.1002/aic.12293.

Song, W., Hess, K.-U., Damby, D.E., Wadsworth, F.B., Lavallée, Y., Cimarelli, C., Dingwell, D.B., 2014. Fusion characteristics of volcanic ash relevant to aviation hazards. Geophys. Res. Lett. 41:2326–2333. http://dx.doi.org/10.1002/2013GL059182.

Song, W., Lavallée, Y., Hess, K.-U., Kueppers, U., Cimarelli, C., Dingwell, D.B., 2016. Volcanic ash melting under conditions relevant to ash turbine interactions. Nat. Commun. 7: 10795. http://dx.doi.org/10.1038/ncomms10795.

Sparks, R.S.J., Walker, G.P.L., 1977. The significance of vitric-enriched air-fall ashes associated with crystal-enriched ignimbrites. J. Volcanol. Geotherm. Res. 2:329–341. http://dx.doi.org/10.1016/0377-0273(77)90019-1.

Steenblik, J.W., 1990. Volcanic ash: a rain of terra. Air Line Pilot 56, 9–15.

Swanson, S.E., Nye, C.J., Miller, T.P., Avery, V.F., 1994. Geochemistry of the 1989–1990 eruption of redoubt volcano: part II. Evidence from mineral and glass chemistry. J. Volcanol. Geotherm. Res. 62:453–468. http://dx.doi.org/10.1016/0377-0273(94)90047-7.

Taltavull, C., Dean, J., Clyne, T.W., 2016. Adhesion of volcanic ash particles under controlled conditions and implications for their deposition in gas turbines. Adv. Eng. Mater. 18:803–813 Special Issue: SPP 1299 – Adaptive Surfaces for High Temperature Applications. http://dx.doi.org/10.1002/adem.201500371.

Taylor, H.E., Lichte, F.E., 1980. Chemical composition of Mount St. Helens volcanic ash. Geophys. Res. Lett. 7:949–952. http://dx.doi.org/10.1029/GL007i011p00949.

Toplis, M.J., Dingwell, D.B., Hess, K.-U., Lenci, T., 1997. Viscosity, fragility, and configurational entropy of melts along the join SiO_2-$NaAlSiO_4$. Am. Mineral. 82:979–990. http://dx.doi.org/10.2138/am-1997-9-1014.

Tupper, A., Guffanti, M., Rose, W., Patia, H., Richards, M., Carn, S., 2007. The "Gulfstream Incident": Twin-engined FLAME-out over the Papua New Guinea Highlands, Fourth International Workshop on Volcanic Ash VAWS/4 WP/07e03.

Vidal-Setif, M.H., Chellah, N., Rio, C., Sanchez, C., Lavigne, O., 2012. Calcium–magnesium–alumino-silicate (CMAS) degradation of EB-PVD thermal barrier coatings: characterization of CMAS damage on ex-service high pressure blade TBCs. Surf. Coat. Technol. 208:39–45. http://dx.doi.org/10.1016/j.surfcoat.2012.07.074.

Vogel, L., Galle, B., Kern, C., Delgado Granados, H., Conde, V., Norman, P., Arellano, S., Landgren, O., Lübcke, P., Alvarez Nieves, J.M., Cárdenas Gonzáles, L., Platt, U., 2011. Early in-flight detection of SO_2 via differential optical absorption spectroscopy: a feasible aviation safety measure to prevent potential encounters with volcanic plumes. Atmos. Meas. Tech. 4:1785–1804. http://dx.doi.org/10.5194/amt-4-1785-2011.

Walker, G.P.L., 1963. The Breiddalur central volcano, eastern Iceland. Q. J. Geol. Soc. 119: 29–63. http://dx.doi.org/10.1144/gsjgs.119.1.0029.

Walsh, P.M., Sayre, A.N., Loehden, D.O., Monroe, L.S., Beer, J.M., Sarofim, A.F., 1990. Deposition of bituminous coal ash on an isolated heat exchanger tube: Effects of coal properties on deposit growth. Prog. Energy Combust. Sci. 16:327–345. http://dx.doi.org/10.1016/0360-1285(90)90042-2.

Watson, I.M., Oppenheimer, C., 2001. Photometric observations of Mt. Etna's different aerosol plumes. Atmos. Environ. 35:3561–3572. http://dx.doi.org/10.1016/S1352-2310(01)00075-9.

Wiesner, M.G., Wang, Y., Zheng, L., 1995. Fallout of volcanic ash to the deep South China Sea induced by the 1991 eruption of Mount Pinatubo (Philippines). Geology 23: 885–888. http://dx.doi.org/10.1130/0091-7613(1995)023<0885:FOVATT>2.3.CO;2.

Witham, C., Webster, H., Hort, M., Jones, A., Thomson, D., 2011. Modelling concentrations of volcanic ash encountered by aircraft in past eruptions. Atmos. Environ. 48: 219–229. http://dx.doi.org/10.1016/j.atmosenv.2011.06.073.

Please cite this article as: Giehl, C., et al., An experimental simulation of volcanic ash deposition in gas turbines and implications for jet engine safety, Chem. Geol. (2016), http://dx.doi.org/10.1016/j.chemgeo.2016.11.024